

University of Groningen

Comparison of methods to study excitation energy transfer in molecular multichromophoric systems

Bondarenko, Anna S.; Knoester, Jasper; Jansen, Thomas L. C.

Published in:
Chemical Physics

DOI:
[10.1016/j.chemphys.2019.110478](https://doi.org/10.1016/j.chemphys.2019.110478)

IMPORTANT NOTE: You are advised to consult the publisher's version (publisher's PDF) if you wish to cite from it. Please check the document version below.

Document Version
Publisher's PDF, also known as Version of record

Publication date:
2020

[Link to publication in University of Groningen/UMCG research database](#)

Citation for published version (APA):

Bondarenko, A. S., Knoester, J., & Jansen, T. L. C. (2020). Comparison of methods to study excitation energy transfer in molecular multichromophoric systems. *Chemical Physics*, 529, [110478]. <https://doi.org/10.1016/j.chemphys.2019.110478>

Copyright

Other than for strictly personal use, it is not permitted to download or to forward/distribute the text or part of it without the consent of the author(s) and/or copyright holder(s), unless the work is under an open content license (like Creative Commons).

The publication may also be distributed here under the terms of Article 25fa of the Dutch Copyright Act, indicated by the "Taverne" license. More information can be found on the University of Groningen website: <https://www.rug.nl/library/open-access/self-archiving-pure/taverne-amendment>.

Take-down policy

If you believe that this document breaches copyright please contact us providing details, and we will remove access to the work immediately and investigate your claim.

Downloaded from the University of Groningen/UMCG research database (Pure): <http://www.rug.nl/research/portal>. For technical reasons the number of authors shown on this cover page is limited to 10 maximum.



Comparison of methods to study excitation energy transfer in molecular multichromophoric systems

Anna S. Bondarenko, Jasper Knoester, Thomas L.C. Jansen

University of Groningen, Zernike Institute for Advanced Materials, Nijenborgh 4, 9747 AG Groningen, The Netherlands

ARTICLE INFO

Keywords:

Multichromophoric aggregates
Excitation energy transfer
HSR
MC-FRET
NISE

ABSTRACT

We compare theoretical methods for calculating excitation energy transfer rates in multichromophoric systems. The employed methods are the multichromophoric Förster resonance energy transfer (MC-FRET), the numerical integration of the Schrödinger equation (NISE), and the Haken-Strobl-Reineker (HSR) model. As a reference, we use the numerically exact Hierarchy of Equations of Motion (HEOM). We examine these methods in various system and bath parameter regimes including the regime relevant to biological light-harvesting systems. We apply them to a model system of a monomeric donor coupled to a multichromophoric acceptor ring of varying size in two limiting configurations, namely symmetric and asymmetric. We find that the symmetric case is more sensitive to the approximations of the methods studied. The NISE method gives the most reasonable results throughout the parameter regimes tested, while still being computationally tractable.

1. Introduction

The role of electronic excitation energy transfer (EET) is of utmost importance in photochemical and photophysical processes in biological and synthetic systems. In the last decades, there has been much interest in understanding the basic mechanisms of EET in systems consisting of organic molecules. Such interest stems from the aspiration not only to gain fundamental knowledge about nature, but also to comply with the technological demand for organic electronic materials. Basic mechanisms for controlled and efficient energy transfer in photosynthetic organisms can, for example, be adopted to design artificial antenna systems or molecular optoelectronic and photonic devices [1–3], photochromic switches [4–6], and molecular sensors [5,7]. A large number of theoretical studies have been performed to elucidate, explain, and characterize the energy transport [8–11]. In assemblies consisting of closely spaced molecules, the EET process is governed by the interplay of the intermolecular interactions in the system itself, giving rise to electronic excited states delocalized over multiple chromophores, and interactions with the noisy environment that inevitably affects the process. For such extended systems, the conventional Förster energy transfer theory does not apply [12] and computationally tractable methods providing reliable results are still not well established, despite the fact that a number of promising methods have been put forward [12–16]. The present work aims to perform a systematic study of the validity, efficiency, and performance of several popular methods to study EET in multichromophoric molecular systems.

The methods we want to evaluate need to contain essential features that have been found to be ubiquitous in natural light-harvesting systems and their synthetic analogues. The natural systems show a large variation in pigment composition, organization, and size, depending on their environments [9] or even light conditions [17,18]. They are typically comprised of tens of pigments, like in the bacterial light-harvesting complexes LH1 [19] and LH2 [20,21], hundreds of pigments, like in photosystems I [22] and II [23,24] of higher plants, or even thousands of pigments, as in the chlorosomes of green sulfur bacteria [25,26]. Synthetic analogues of light-harvesting systems obtained by self-assembly of organic dye molecules such as meso-tetra(4-sulfonatophenyl) porphyrin (TPPS4) [27], the cyanine dye 3,3'-bis(2-sulfo-propyl)-5,5',6,6'-tetrachloro-1,1'-diocetylbenzimidacarbocyanine (C8S3) [28–30], and zinc chlorin (ZnChl) [31] are usually composed of a large number (many thousands) of pigments. Theoretical methods designed to describe EET within and between such systems, should be able to deal with many strongly coupled chromophores with good accuracy in a reasonable computational time.

Optically relevant excited states in molecular aggregates are typically described as Frenkel excitons, i.e., neutral collective electronic excitations which are superposition states of the excited states of individual molecules within the assembly. Due to strong intermolecular interactions, the electronic excitations are coherently shared between a number of molecules in the aggregate. In the absence of disorder, these excitons are delocalized throughout the whole aggregate. In the regime of weak interactions with vibrations, the EET is initially coherent in

E-mail addresses: j.knoester@rug.nl (J. Knoester), t.l.c.jansen@rug.nl (T.L.C. Jansen).

<https://doi.org/10.1016/j.chemphys.2019.110478>

Received 27 May 2019; Received in revised form 11 August 2019; Accepted 11 August 2019

Available online 26 August 2019

0301-0104/ © 2019 The Authors. Published by Elsevier B.V. This is an open access article under the CC BY license (<http://creativecommons.org/licenses/by/4.0/>).

time, i.e., characterized by back and forth oscillations. The excitation thus propagates like a wave packet. In the regime of strong coupling to a bath of vibrations, phase relations decay rapidly in time, and the exciton motion takes place through an incoherent hopping process. A proper theoretical description should be able to account for both the coherent transport between strongly coupled chromophores and the incoherent transport between weakly coupled chromophores.

The theory of Förster resonance energy transfer (FRET) [32] has been successfully applied to EET between two weakly coupled chromophores – a donor and an acceptor – in the regime of incoherent energy transfer. It expresses the EET rate in terms of the overlap integral between the emission spectrum of the donor and the absorption spectrum of the acceptor. FRET, which is highly distance-dependent, became a popular tool to probe intermolecular distance in complex systems [33]. Despite its utility, the Förster theory fails when the donor and/or the acceptor system is an aggregate of strongly interacting chromophores and the donor-acceptor distance is comparable to the physical size of the aggregate. In this case, the donor-acceptor interaction can not be treated in the dipole approximation and EET may occur between optically forbidden exciton states. An extension of the Förster theory to multichromophoric donor and/or acceptor systems constitutes one set of methods that we will consider here. This is known as Multichromophoric Förster Resonance Energy Transfer (MC-FRET) theory and was first proposed by Sumi [12], and later further developed and evaluated by Jang et al. [34], Scholes and Fleming [35], Giorda et al. [36], and Cao et al. [37–40]. In this theory, distances between neighboring molecules within the donor and acceptor aggregates are assumed to be smaller than the closest separation between molecules of the two aggregates considered, but this latter separation is not necessarily larger than the size of the individual aggregates. Such arrangement gives rise to strong couplings within the donor and/or acceptor complexes, leading to delocalized excitonic states within these respective systems, while the weak donor-acceptor coupling still allows for a perturbative treatment of the EET process between the two complexes, albeit it not in the dipole approximation for the aggregates. An important advantage of the MC-FRET method is its ability to incorporate both memory effects and thermal relaxation in the bath description. As a consequence, the Stokes shift is included explicitly, which is important to properly describe the EET from the donor to the acceptor system. The main limitation of the MC-FRET is its restriction to the perturbative limit of the EET process, i.e., the donor-acceptor coupling must be weak compared to the interaction with the bath, and the EET process between the donor and acceptor aggregates must follow an incoherent hopping mechanism.

One of the most acclaimed models describing all regimes between coherent and incoherent motion in molecular aggregates is the Haken-Strobl-Reineker (HSR) model [13,41], which models the effect of the bath as classical fluctuations of the molecular transition energies and the intermolecular excitation transfer interactions. Its popularity originates in its simplicity. As MC-FRET, it is also capable of describing multichromophoric systems, but does not treat the donor-acceptor interaction perturbatively and is, therefore, not limited to the weak donor-acceptor coupling regime. The major limitation of the HSR model lies in its restriction to fast fluctuations of the bath as it assumes the white noise limit, and its intrinsic high-temperature limit. Importantly, the HSR model is able to describe the crossover between coherent and incoherent energy transfer.

In contrast to the HSR model, the Numerical Integration of the Schrödinger Equation (NISE) method [14,42], where the time-dependent Schrödinger equation is explicitly solved and averaged over explicit bath trajectories, properly incorporates the description of the bath from fast to slow modulation limits, yet preserving simplicity in its implementation. It is also capable of describing the multichromophoric nature of the aggregate system and has no restriction on the donor-acceptor coupling. As the method neglects the effect of the system on the bath, it gives a thermal realization that corresponds to the high-

temperature limit [43].

Finally, a formally exact numerical method describing coupled coherent-incoherent motion with a correct description of the effect of the system on the bath is the Hierarchy of Equations of Motion (HEOM) [44–46]. It is based on the stochastic Liouville approach where the system's density matrix is coupled to a hierarchy of auxiliary density matrices that accounts for a non-Markovian system-bath coupling. HEOM has become the “gold standard” against which other approximate methods can be compared. However, unfavorable computational scaling with the system size makes it unappealing for studying molecular systems larger than around 50 molecules [46].

In this paper, we compare the above theoretical methods for studying the EET in molecular aggregates and provide guidelines on the limits of their applicability and performance. We apply these methods to model systems of a monomeric donor coupled in two configurations to a multichromophoric molecular acceptor ring of varying size. We consider a wide range of parameters describing the system, the bath, and the system-bath coupling that includes both limiting cases and parameters comparable to those found in natural light-harvesting systems. We use HEOM as a reference for those parameter sets where the high-temperature approximation may fail.

The outline of the remainder of this paper is as follows. In Section 2, we present the model system, while in Section 3, we describe the pertinent details of the methods for calculating EET that we compare. In Section 4, we present and discuss the results of these methods applied to a monomeric donor coupled to a multichromophoric acceptor ring of varying size. Finally, in Section 5, we present our conclusions.

2. Model system

We will use the general framework of Frenkel excitons [47,48] to describe the energy transfer in molecular aggregates. For simplicity, we will limit our treatment in this paper to the energy transfer from one molecule (donor) to a complex of strongly interacting molecules (acceptor). All molecules are treated as two-level systems, with a ground state and an optically accessible excited state. The full system is then described by the following Hamiltonian:

$$H(t) = H^D(t) + H^A(t) + J^{D-A}, \quad (1)$$

where the Hamiltonians $H^D(t)$ and $H^A(t)$ characterize the donor molecule and the acceptor complex, respectively, and J^{D-A} describes the interaction between them. In our study, $H^D(t)$, is given by:

$$H^D(t) = (\epsilon^D + \delta \epsilon^D(t)) a^\dagger a, \quad (2)$$

where ϵ^D is the electronic transition energy of the donor molecule and $\delta \epsilon^D(t)$ is the time-dependent fluctuation in this energy that accounts for the interaction with the (thermal) environment; $a^\dagger(a)$ denotes the Pauli creation (annihilation) operator for an excitation on the molecule.

The Hamiltonian of the acceptor complex, $H^A(t)$, is represented by the Frenkel exciton Hamiltonian [47,48]:

$$H^A(t) = \sum_n (\epsilon^A + \delta \epsilon_n^A(t)) b_n^\dagger b_n + \sum_{n \neq m} J_{nm}^A b_n^\dagger b_m, \quad (3)$$

where $b_n^\dagger(b_n)$ denotes the Pauli creation (annihilation) operator for an excitation on acceptor molecule n . The summations over n and m run over all molecules (1, 2, ..., N_A) in the acceptor complex. Furthermore, ϵ^A is the average transition energy, which in this study is assumed equal for all acceptor molecules, and $\delta \epsilon_n^A(t)$ indicates the fluctuation in the transition energy for molecule n caused by the interaction with the environment. These fluctuations are assumed uncorrelated for different molecules. Finally, J_{nm}^A is the electronic coupling between molecules n and m , which for the sake of simplicity is treated as a constant (no fluctuations); for several light-harvesting complexes this has been shown to be a reasonable approximation [49–51]. In the absence of fluctuations, the acceptor's one-quantum excited eigenstates are Frenkel excitons with energies E_k^A that result from diagonalizing H^A

with $\delta \epsilon_n^A = 0$.

The last term of Eq. (1) describes the electronic couplings between the donor and acceptor molecules:

$$J^{D-A} = \sum_n J_n^{D-A} b_n^\dagger a + J_n^{D-A*} a^\dagger b_n. \quad (4)$$

The electronic couplings in Eq. (3) and (4) can be calculated within the point-dipole approximation [52], multipole approximation [52], extended dipole approximation [53,54], or the transition charge electrostatic potential (TrEsp) method [55,56]. For our purpose of method comparison we will treat the couplings phenomenologically. In particular, within the acceptor ring to be considered, we restrict ourselves to nearest-neighbor interactions.

We will consider two specific system geometries, one in which the donor is at the center of a circular acceptor aggregate and one in which the donor resides outside such a circular aggregate (see Section 4).

3. Methods for calculating the EET rate

In this section, we describe how in the methods considered, the bath is incorporated and the rate is obtained. In order to keep the paper reasonably self-contained and ensure proper translation of parameters between methods, for each method essential details are discussed. Their limitations will be summarized in Table 1.

3.1. General considerations

In the MC-FRET method, the EET rate constant between a donor molecule and an acceptor aggregate is directly calculated from the spectral overlap integrals, as will be described in detail later. By contrast, in the NISE, HSR, and HEOM methods, one calculates the probabilities for the excitation to reside on a particular (donor or acceptor) molecule as a function of time t , after placing it at the donor molecule at $t = 0$, and the EET rate constant is then extracted from the time dependence of these probabilities. In this subsection, we show how we do this.

In this study, we only consider the regime of incoherent energy transfer from a single donor molecule to the acceptor complex. In this case, initially coherent oscillations between the donor and acceptor states are damped fast on the scale of donor-acceptor EET, due to the interaction with the bath of vibrations and the EET may effectively be described through incoherent rate equations. In general, for the probability $P_D(t)$ for the donor molecule to be excited, this results in a short-time plateau, possibly with small oscillations, followed by multi-exponential decay to the multichromophoric acceptor. In this paper, we are particularly interested in the situation where the resonance interactions within the acceptor complex are much larger than the donor-acceptor interactions. In practice, this implies that equilibration of excitations within the acceptor complex occurs much faster than the EET

from the donor to the acceptor complex. As a consequence, the acceptor may be described as one effective site, with excitation probability $P_A(t) = 1 - P_D(t)$ and the excitation probability is governed by one simple rate equation only:

$$\frac{dP_D(t)}{dt} = -kP_D(t) + k'(1 - P_D(t)), \quad (5)$$

where k is the total EET from the donor molecule to the acceptor ring and k' is the backtransfer rate. Eq. (5) gives rise to single-exponential decay, which indeed in all our simulations is observed (after the short-time transient behavior). The rate k in Eq. (5) is the EET we are after in this study and the quantity that should be compared to the rate obtained from the MC-FRET method. In the following, we describe how k can be extracted from $P_D(t)$ as computed through the other methods.

First, it is important to note that k and k' are time-independent rates. Hence, they are related through $kP_D^{eq} = k'(1 - P_D^{eq})$, where P_D^{eq} is the donor excitation probability in equilibrium, i.e., at long times. Thus, $k' = kP_D^{eq}/(1 - P_D^{eq})$. Substituting this into Eq. (5) and solving for $P_D(t)$ yields

$$P_D(t) = P_D^{eq} + (1 - P_D^{eq})e^{-k_{eff}t}. \quad (6)$$

Hence, $k_{eff} = k/(1 - P_D^{eq})$ is the effective rate of the single-exponential decay observed for $P_D(t)$. Thus, the procedure followed to obtain the rate k from the HSR, NISE, or HEOM methods, is to fit their respective results to Eq. (6), from which values for P_D^{eq} and k_{eff} are obtained. From this, we calculate the total EET from the donor to the acceptor complex as $k = (1 - P_D^{eq})k_{eff}$.

In the limit of high temperature, always applicable to the HSR and NISE methods, as these are intrinsically giving high-temperature equilibrium conditions, we have $P_D^{eq} = (N_A + 1)^{-1}$, implying that $k = k_{eff}N_A/(N_A + 1)$.

3.2. Treatment of the thermal bath

The thermal noise of the bath is crucial for the EET process. In the following, we discuss how each of the methods for calculating the EET rate incorporates a noise correlation function. To limit the number of free parameters in the description of the bath, we will employ the overdamped Brownian oscillator model [57]. The bath vibrations are then modeled as a collection of independent harmonic oscillators and the system-bath coupling is assumed to be bilinear in system and bath frequency coordinates. The spectral density of this overdamped model is then given by [57]:

$$D(\omega) = 2\lambda \frac{\omega\Lambda}{\omega^2 + \Lambda^2}, \quad (7)$$

where λ is the reorganization energy characterizing the coupling strength of the bath fluctuations to the electronic transition and Λ is the inverse of the correlation time of the bath fluctuations: $\Lambda = 1/\tau_c$.

The different EET methods employed here utilize different approximations for the bath. In essence, this is related to describing the effect of the bath on the optical line shape of the molecular systems considered at different levels of approximation. The interaction with the bath results in broadening of these line shapes, thus affecting the spectral overlap between the emission line shape of the donor and the absorption line shape of the acceptor complex. Below, we will specify these different approximations. The MC-FRET methods allow to use line shapes based on the full quantum time-correlation function. Within the fluctuation-dissipation theorem, which relates the response function to the correlation function, and using the second-order cumulant expansion, all the necessary information to calculate the optical response function is carried in the quantum time-correlation function $C^q(t)$ [57,58]. In general, it is complex and is expressed by [57,59,60]:

$$C^q(t) = \frac{1}{\pi} \int_0^\infty d\omega D(\omega) \left\{ \coth\left(\frac{\hbar\omega}{2k_B T}\right) \cos(\omega t) - i \sin(\omega t) \right\}, \quad (8)$$

Table 1

Summary of the limitations of the methods considered in this work. “–” means no restrictions are imposed by the method, ΔW is the exciton bandwidth, J^{D-A} is the largest donor-acceptor coupling.

Method	Temperature	Bath fluctuations	Coupling strength
MC-FRET ^{IAL}	–	$\kappa \gg 1^\dagger$	$\Gamma \gg J^{D-A}$
MC-FRET ^{diag}	–	–	$\Gamma \gg J^{D-A}$
MC-FRET ^{diag, IPR}	–	–	$\Gamma \gg J^{D-A}$
NISE	$k_B T \gg \hbar\Lambda$, $k_B T \gg \Delta W$	no Stokes shift	–
HSR	$k_B T \gg \hbar\Lambda$, $k_B T \gg \Delta W$	$\kappa \gg 1$, no Stokes shift	–
HEOM	–	–	–

[†] As follows from the unreasonable line shape when κ is of the order of unity or smaller (see Section 4.2).

where $D(\omega)$ is the spectral density of the harmonic bath, which in our case is given by Eq. (7). The imaginary part of Eq. (8) accounts for the Stokes shift.

The effect of the bath in the NISE method is accounted for by a stochastic model known as the overdamped Brownian oscillator. It assumes that the classical heat bath randomly pushes the system, thereby, affecting the molecular excitation energies of the system, expressed by the fluctuating terms $\delta \epsilon^D(t)$ and $\delta \epsilon_n^A(t)$ of Eqs. (2) and (3). Here, the influence of the system on the bath is neglected and as a result the Stokes shift is completely omitted. For the Brownian oscillators, the stochastic process is Gaussian with mean zero ($\langle \delta \epsilon(t) \rangle = 0$) and two-time correlation functions given by [57]:

$$C(t) = \langle \delta \epsilon(t) \delta \epsilon(0) \rangle = \sigma^2 \exp(-\Lambda t), \quad (9)$$

where the angular brackets $\langle \dots \rangle$ indicate averaging over the stochastic process and $\delta \epsilon$ generically indicates the energy fluctuation on any of the molecules; correlations in these fluctuations between different molecules are neglected. Here, σ indicates the root-mean-squared amplitude (or magnitude) of the energy fluctuations, which may be related to the reorganization energy and temperature by taking the classical limit [57] of Eq. (8) for $k_B T \gg \Lambda$:

$$\sigma^2 = \frac{2\lambda k_B T}{\hbar}. \quad (10)$$

This allows us to translate the reorganization energy and temperature of the MC-FRET method to the fluctuation amplitude in the NISE method.

The HSR model also uses the Gaussian stochastic process described above, but assumes the correlation time of the bath fluctuations, Λ^{-1} , to be infinitely short. In other words, the bath fluctuations have a white noise spectrum. Physically, this implies that the frequency distribution of the vibrations is significantly broader than the exciton bandwidth. In this case, the correlation function of Eq. (9), $C(t)$, reduces to

$$C^{wn}(t) = \langle \delta \epsilon(t) \delta \epsilon(0) \rangle = \frac{\sigma^2}{\Lambda} \delta(t), \quad (11)$$

where the ratio σ^2/Λ can be expressed as a single parameter, known as the homogeneous line width:

$$\Gamma \equiv \frac{\sigma^2}{\Lambda} = \frac{2\lambda k_B T}{\hbar \Lambda}. \quad (12)$$

This situation corresponds to the fast modulation limit in line shape theory [58], giving rise to a Lorentzian line shape of the optical spectrum of single molecules with a full-width at half-maximum (FWHM) of 2Γ . The value of Γ corresponding to the bath used in MC-FRET and NISE can be determined from Eq. (12).

A convenient dimensionless parameter, κ , is used for characterizing the speed of the dynamics of the bath [58]:

$$\kappa = \frac{\Lambda}{\sigma} = \sqrt{\frac{\hbar \Lambda^2}{2\lambda k_B T}}. \quad (13)$$

In the fast modulation limit, the bath fluctuations are fast compared to the bath coupling strength, and thus $\kappa \gg 1$. In the slow modulation limit, the opposite holds. The line shape of the optical spectrum evolves from a Lorentzian with no Stokes shift for $\kappa \ll 1$ to a Gaussian with a Stokes shift of 2λ for $\kappa \gg 1$. In the intermediate regime, the line shape is described by a Voigt profile [57].

In the remainder of this section, we explain how in each method considered, the EET dynamics within the coupled donor-acceptor system described by the Hamiltonian in Eq. (1) and with the bath treatments given above, is evaluated.

3.3. Multichromophoric Förster resonance energy transfer (MC-FRET)

The equation for the MC-FRET rate constant derived in Ref. [12] has the form:

$$k^{\text{MC-FRET}} = \frac{2\pi}{\hbar} \int d\omega \text{Tr}^{(D)}[(J^{D-A})^\dagger I^A(\omega) J^{D-A} E^D(\omega)], \quad (14)$$

where $I^A(\omega)$ is the absorption matrix of the acceptor complex spanned by the electronic excited states in the acceptor, $E^D(\omega)$ is the emission matrix of the donor complex spanned by the electronic excited states on the donor, and $\text{Tr}^{(D)}$ denotes the trace over the electronic excited states on the donor. $I^A(\omega)$ and $E^D(\omega)$ represent the density of states (DOS) in the acceptor and donor, respectively. They are determined by the thermal averaging over a bath of vibrations and do not include transition dipole moments in their expressions. For our monomeric donor, the emission matrix $E^D(\omega)$ is reduced to a scalar giving the emission spectrum. J^{D-A} denotes the electronic coupling between the donor and the acceptor complex as defined by the first term in Eq. (4) and $(J^{D-A})^\dagger$ is its transpose, i.e., the second term of Eq. (4). As can be seen from Eq. (14), the MC-FRET rate constant is determined by the overlap between $I^A(\omega)$ and $E^D(\omega)$. The influence of the coupling between the bath of vibrations and the system is captured in the position and width of the spectral peaks. The absorption matrix and the emission spectrum used in the MC-FRET equation can be obtained through different approximations as discussed below.

Within the second-order cumulant approximation, the emission spectrum of the monomeric donor is given by [57]:

$$E^D(\omega) = \frac{1}{\pi} \text{Re} \int_0^\infty dt e^{i(\omega - \epsilon^D)t - g^*(t)}, \quad (15)$$

where the line broadening function $g(t)$ is derived from the quantum correlation function of Eq. (8), giving the equation [57]

$$g(t) = \frac{1}{\pi} \int_0^\infty d\omega \frac{1 - \cos(\omega t)}{\omega^2} \coth\left(\frac{\hbar\omega}{2k_B T}\right) D(\omega) - \frac{1}{\pi} \int_0^\infty d\omega \frac{i \sin(\omega t) - \omega t}{\omega^2} D(\omega). \quad (16)$$

with $D(\omega)$ the spectral density as defined in Eq. (7).

For the multichromophoric acceptor system, in general, there is no simple expression for the absorption line shape. Below we consider three commonly used approximations that will define different ways to obtain the MC-FRET rates.

The first approximation considered uses the ideal absorption line shape (IAL) [59,60] and is labeled MC-FRET^{IAL}. The expression for the IAL is based on the quantum master equation formalism and without quasistatic disorder has the form:

$$I^A(\omega) = -\frac{1}{\pi} \text{Im} \left\{ \frac{1}{\omega + (E_g - H_0^A)/\hbar + i\hat{\mathcal{K}}(\omega)} \right\}, \quad (17)$$

where H_0^A is the unperturbed exciton Hamiltonian of the acceptor complex, i.e., Eq. (3) without the fluctuating term in the transition energies, $\delta \epsilon_n^A = 0$. The interaction with the bath, which results in finite $\delta \epsilon_n^A$ and in broadening of the line shape, is characterized by the dissipation kernel $\hat{\mathcal{K}}(\omega)$ defined as [59]:

$$\hat{\mathcal{K}}(\omega) = \sum_{n=1}^{N_A} \sum_{k=1}^{N_A} \hat{C}^q(\omega - E_k^A/\hbar) |c_k^n|^2 b_n^\dagger b_n, \quad (18)$$

where E_k^A and c_k^n are the eigenvalues and the eigenvector coefficients of H_0^A , respectively, and $\hat{C}^q(\omega)$ is the frequency domain correlation function obtained from the one-sided Fourier transform of $C^q(t)$, defined in Eq. (8):

$$\hat{C}^q(\omega) = \int_0^\infty dt e^{i\omega t} C^q(t), \quad (19)$$

The second approximation considered is the so-called diagonal (secular) MC-FRET approximation [35,60,61], also referred to as the generalized Förster rate, labeled here MC-FRET^{diag}. It is based on the assumption that the acceptor absorption density operators are diagonal in the eigenbasis. This means that the bath fluctuations are not large

enough to considerably scramble the exciton basis. Therefore, the expression for the rate constant in Eq. (14) includes the acceptor-donor coupling in the eigenstate basis:

$$J_k = \sum_{n=1}^{N_A} J_n^{D-A} c_k^{n*}, \quad (20)$$

and the following expression for the diagonal elements of the absorption matrix:

$$I_{kk}^A(\omega) \approx 2\text{Re} \int_0^\infty dt e^{i(\omega - E_k^A)t - g(t)}, \quad (21)$$

where $g(t)$ is a single molecule line broadening function, which is assumed to be the same as for the donor molecule in Eq. (16).

The third approximation takes into account exchange narrowing in the acceptor complex, i.e., the fact that the electronic couplings reduce the line width of a coupled multichromophoric system compared to a single chromophore [62–64]. The exchange narrowing effect is well known for J-aggregates in the limit of static disorder [65]. Taking the exchange narrowing effect into account, we obtain the inverse participation ratio (IPR) MC-FRET approximation [66], labeled MC-FRET^{IPR}, which uses the eigenstate absorption line shape of Eq. (21) scaled by the corresponding participation ratio of the eigenstates:

$$I_{kk,IPR}^A(\omega) \approx 2\text{Re} \int_0^\infty dt e^{i(\omega - E_k^A)t - \mathcal{P}_k^A g(t)}, \quad (22)$$

where $\mathcal{P}_k^A = \sum_n |c_n^k|^4$ is the participation ratio [65,67] of the state k in the acceptor complex. Without static disorder, as is the case for our calculations, \mathcal{P}_k^A is in the order of $1/N_A$.

In essence, the three MC-FRET methods outlined above should be applicable for any time scale of the bath dynamics, given that the line shape is valid, i.e., for all values of κ . The temperature and the Stokes shift are included explicitly in the method. The biggest limitation of the method is its restriction to the perturbative treatment of the donor-acceptor interaction, implying only incoherent energy transfer from the donor to the acceptor system. The computational effort (CPU time) for the three MC-FRET methods all scale approximately as $O(N_A^3)$ with the system size as they all require the diagonalization of the acceptor Hamiltonian and otherwise involve inversion of matrices of size $N_A \times N_A$.

3.4. Numerical integration of the Schrödinger equation (NISE)

In the NISE method [14,42], the dynamics is modeled explicitly averaging over trajectories using wave function theory. The dynamics of the system is determined by the time-dependent Schrödinger equation:

$$\dot{\Psi}(t) = -\frac{i}{\hbar} H(t) \Psi(t), \quad (23)$$

where $\Psi(t)$ is the exciton wave function at time t . This equation is solved numerically by dividing time into small intervals, Δt (with $\Delta t \ll \Lambda^{-1}$), and solving the Schrödinger equation for each interval assuming the Hamiltonian to be constant over it:

$$\Psi(t + \Delta t) = U(t + \Delta t, t) \Psi(t), \quad (24)$$

where $U(t + \Delta t, t)$ is the time-evolution matrix:

$$U(t + \Delta t, t) = \exp\left(-\frac{i}{\hbar} H(t) \Delta t\right). \quad (25)$$

Here, $H(t)$ is the Hamiltonian which parametrically depends on the time-evolution of the classical bath coordinates. The time-evolution for longer times is obtained through multiplying consecutive time-evolution matrices, leading to the expression:

$$U(t, 0) = \prod_{j=1}^{t/\Delta t} U(j\Delta t, (j-1)\Delta t). \quad (26)$$

The effect of the bath on the system is accounted for by the stochastic fluctuations $\delta \epsilon^D(t)$ and $\delta \epsilon_n^A(t)$ in Eqs. (2) and (3), respectively, characterized by Eq. (9). To this end, we construct the Hamiltonian trajectories in the following way [68]:

$$\delta \epsilon(t + \Delta t) = \delta \epsilon(t) \exp(-\Delta t \Lambda) + G(\sigma) \sqrt{1 - \exp(-2\Delta t \Lambda)}, \quad (27)$$

where $G(\sigma)$ is a random number taken from a Gaussian distribution with width σ and mean zero. At the first time step the fluctuating molecular frequencies are initialized as random numbers from a Gaussian distribution with width σ and mean zero.

In the NISE method, we monitor the population transfer between the donor molecule and the acceptor complex through the decay of the population of the donor:

$$P_D(t) = |\langle \Psi_D | U(t, 0) | \Psi_D \rangle|^2, \quad (28)$$

where Ψ_D is the state in which the donor is excited. To obtain the results reported in Section 4, we averaged over 50 000 random realizations of the Hamiltonian trajectories. The rate constant can be obtained by analyzing the population transfer, as discussed in Section 3.1 (Eq. (6)).

The main advantages of the NISE method are its simplicity in implementation and the ability to properly incorporate colored noise, i.e., to use arbitrary values of κ . The most important disadvantages of the NISE method are its intrinsic high-temperature limit ($k_B T \gg \hbar \Lambda$ and $k_B T \gg \Delta W$, where ΔW is the exciton bandwidth), resulting in an equilibrium state of equal probability for all exciton states, and the neglect of the Stokes shift as a result of the omission of the imaginary part in the bath correlation function. The computation time for the NISE method scales as $O(N_A^3)$ with the system size, because the most time-consuming part of the calculation is determining the matrix exponentials in Eq. (25). A comparison of alternative propagation schemes can be found in Ref. [69]. Another drawback is that the calculations have to be repeated for many disorder realizations in order to obtain an average over the bath fluctuations.

3.5. Haken-Strobl-Reineker (HSR) model

The HSR model [13,41] is based on the stochastic Liouville equation (SLE) description of coupled coherent and incoherent exciton dynamics [41]. The coherent part of the dynamics is characterized by the unperturbed Hamiltonian H_0 , i.e., Eq. (1) without fluctuations in the molecular transition energies. The incoherent part results from these fluctuations which, as stated above, are treated as Gauss-Markov stochastic processes described by Eqs. (11) and (12). The equation of motion for the density matrix element ρ_{nm} is then given by [13]:

$$\frac{d}{dt} \rho_{nm} = -\frac{i}{\hbar} [H_0, \rho]_{nm} - 2\Gamma(1 - \delta_{nm}) \rho_{nm}(t), \quad (29)$$

where n is a generic label for a molecule (either donor or any acceptor molecule). In this approach, the excited-state phase relations between two molecules decay with rate 2Γ , which destroys the back and forth oscillations in the occupation probabilities ρ_{nn} of individual molecules, either on a time step fast compared to EET between both molecules involved (incoherent limit, $J_{nm} \ll \Gamma$) or slow ($J_{nm} \gg \Gamma$).

The main advantage of the HSR model is its simplicity in implementation. However, like the NISE method, a major limitation of the HSR model is its high-temperature limit: $k_B T \gg \hbar \Lambda$ and $k_B T \gg \Delta W$. Furthermore, the HSR model is naturally limited to the fast fluctuation limit, $\kappa \gg 1$. The computation effort for the HSR model scales approximately as $O(N_A^6)$ with the system size, because it requires propagating the density matrix. However, in contrast to the NISE method, all the dynamic disorder is automatically included and no additional averaging over realizations of the fluctuations is needed as long as only dynamic disorder is considered.

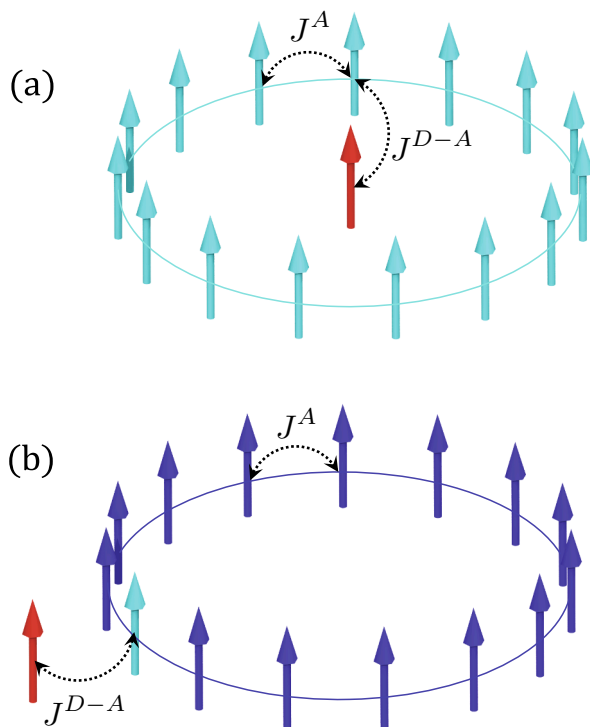


Fig. 1. Graphical representation of the two model systems considered. In each case, the model consists of an acceptor ring (light blue or blue) and a monomeric donor (red) with transition dipoles oriented perpendicularly to the plane of the ring. In the symmetric system (a), the donor is placed in the center of the ring and is coupled to each of the acceptor molecules (light blue) resulting in equal couplings, $J^{D-A} = J$ for all donor-acceptor pairs. In the asymmetric system (b), the donor is placed outside of the ring and is coupled only to the nearest acceptor molecule with strength $J^{D-A} = J$ (light blue); no coupling exists with the rest of the acceptor molecules (blue).

3.6. Hierarchy of Equations of Motion (HEOM)

The HEOM method is based on the exact equations of motion for a system with bilinear coupling to a quantum-mechanical harmonic oscillator bath. A description of the implementation of this method for a bath of overdamped Brownian oscillators can be found in Ref. [46]. The method is numerically exact as long as the bath can be described by a

spectral density of independent quantum harmonic oscillators.

We use the PHI software package [46,70] to calculate HEOM exciton dynamics and obtain $P_D(t)$, from which the EET rate constant was extracted (see Section 3.1). For the system parameters studied here, it turned out not necessary to include Matsubara frequencies [15]. We use a hierarchy depth of 11, which was tested for convergence by comparing to results with higher hierarchy depth.

4. Results and discussion

In this study, the acceptor complex is a ring with the number of molecules, N_A , ranging from 1 to 20 and the molecular transition dipoles oriented perpendicularly to the plane of the ring (Fig. 1). Such configuration of transition dipoles corresponds to an H-type aggregate. Within this ring, only nearest-neighbor electronic interactions, $J^A (> 0)$, are considered. We consider two locations for the molecular donor: (a) “symmetric system”, where the donor is placed in the center of the ring (Fig. 1a), resulting in equal couplings for all donor-acceptor pairs, $J_n^{D-A} = J$; (b) “asymmetric system”, where the donor is placed outside the ring (Fig. 1b) and is coupled only to the nearest acceptor molecule, again with coupling strength denoted as J . These configurations resemble typical chromophore arrangements as found for transfer within and between natural light-harvesting aggregates, while preserving a high degree of simplicity to ease the interpretation and facilitate comparison of the methods considered. The parameters are chosen to ensure a strongly delocalized acceptor system and a weak coupling between the donor and the acceptor system. All energetic quantities are expressed in units of the electronic donor-acceptor coupling J . Furthermore, we either use $\epsilon^D = \epsilon^A$ (unbiased case) or $\epsilon^D = \epsilon^A + \Delta E$ (biased case).

In the following subsections, we present and discuss the results for different regimes of the system and bath parameters, all of which are summarized in Table 2.

4.1. High-temperature and fast-modulation limit

First, we consider the limit of high temperature ($k_B T \gg \hbar \Lambda$, $k_B T \gg \Delta W$) and fast modulation dynamics ($\kappa \gg 1$). In this range, all methods are expected to work well and thus agree with each other. We examine this for the example of the symmetric unbiased donor-acceptor system with $N_A = 4$ (Fig. 1a). In Fig. 2, the rate constant, calculated with the different methods, are presented as a function of κ . As can be seen from the plot, all methods apart from the MC-FRET^{diag}, IPR agree. The discrepancy for the MC-FRET^{diag}, IPR is attrib-

Table 2

System and bath parameters used in the calculations: the nearest-neighbor coupling in the acceptor (J^A), the donor-acceptor coupling (J^{D-A}), the number of molecules in the acceptor ring (N_A), the temperature ($k_B T$), the inverse of the correlation time (Λ), and the reorganization energy (λ).

Regime	System parameters			Bath parameters		
	J^A (J)	J^{D-A} (J)	N_A	$k_B T$ (J)	Λ (J)	λ (J)
<i>High-temperature, fast-modulation limit (Section 4.1)</i>						
Function of κ (Fig. 2)	10	1	4	5000	500	0.2–10
Size dependence (Fig. 3)	10	1	1–20	5000	500	0.2
<i>High-temperature, slow-modulation limit (Section 4.2)</i>						
Function of κ (Fig. 4)	10	1	4	5000	10–500	1
Size dependence (Fig. 6)	10	1	1–20	5000	40	1
Stronger coupling in A (Fig. 7)	150	1	1–20	5000	40	1
Asymmetric system (Fig. 8)	150	1	1–20	5000	40	1
	J^A (cm ⁻¹)	J^{D-A} (cm ⁻¹)	N_A	$k_B T$ (cm ⁻¹)	Λ (cm ⁻¹)	λ (cm ⁻¹)
<i>Intermediate regime (Section 4.3)</i>						
Real system parameters (Fig. 9a and 10a)	300	20	1–20	200	333.6	100
High temperature (Fig. 9b and 10b)	300	20	1–20	5000	333.6	100
High temperature, small λ (Fig. 9c and 10c)	300	20	1–20	5000	333.6	4

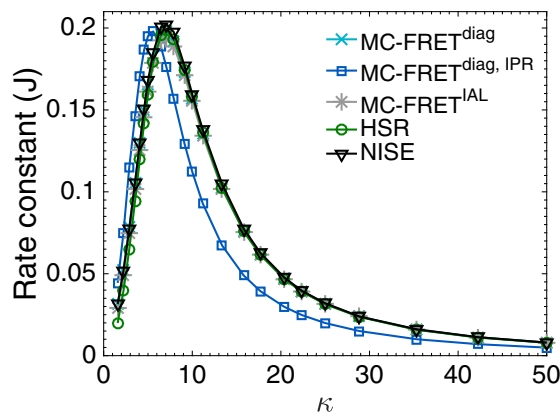


Fig. 2. Rate constant for the donor-acceptor energy transfer in the symmetric system with $J^A = 10 J$, $J^{D-A} = J$, and $N_A = 4$ as a function of κ in the limit of high temperature and fast dynamics: $k_B T = 5000 J$, $\Lambda = 500 J$. The reorganization energy λ is varied from 0.01 to 10 J, resulting in κ ranging from 1.58 to 50. No donor-acceptor energy bias was included.

uted to the fact that the effect of the exchange narrowing, taken into account by a simple scaling of the line shape using the participation ratio, is considerably overestimated by using the IPR for the ordered acceptor system. While it was shown that the effect of exchange narrowing, often seen in the static-disorder limit, is also found in the fast fluctuation limit [71], the effect is not as prominent as it is in the static-disorder limit. Closer inspection of the graph reveals that the rate constant calculated with the HSR model (green curve) deviates slightly as κ decreases. This behavior is expected, because smaller κ corresponds to slower dynamics, i.e., moving out of the validity regime of the HSR model.

We note that the current high-temperature, fast-fluctuation limit case serves as a good validation of the implementation of the different methods.

The fact that the maximum rate constant is reached at finite κ ($\kappa \approx 7$) can be explained in terms of the optimal overlap between the emission line shape of the donor molecule and the line shape corresponding to the absorption matrix of the acceptor complex. When κ is too large, the line widths become too narrow, resulting in partial overlap. As κ decreases, the width gets larger, as does the overlap, thereby resulting in a large rate constant. This overlap will reach an optimum however, because when the line shapes become too broad, the absolute value of the overlap gets smaller again, because the peak heights decrease.

We now consider the effect of the size of the acceptor system on the rate constant for one fixed value of $\kappa = 11.2$, again for the symmetric unbiased donor-acceptor system, and compare all methods to the HEOM standard (Fig. 3). As can be seen, all methods apart from the MC-FRET^{diag, IPR}, are in excellent agreement. The deviation for the MC-FRET^{diag, IPR}, as discussed previously, is attributed to the overestimation of the effect of exchange narrowing. Due to the symmetry, the accepting state of the acceptor complex considered here is predominantly the totally symmetric ($k = 0$) exciton state, which for an H-aggregate is the state with the highest energy. For the unbiased donor-acceptor system, the overlap between the donor emission line shape and the absorption line shape for $N_A = 1$ is maximal, because the monomer energy of the donor and acceptor is the same and there is no Stokes shift. The overlap decreases for $N_A = 2, 3$ due to the lower overlap between the monomer donor line shape and the excitonic acceptor states, because the latter split and the accepting state lies higher in energy than the donor excited state. When N_A increases beyond 4, the energy of the excitonic acceptor state that overlaps with the donor state hardly changes anymore and the rate constant only depends on the donor-acceptor coupling which increases linearly with N_A . This results in the linear behavior for the rate constant beyond $N_A = 4$ observed in Fig. 3.

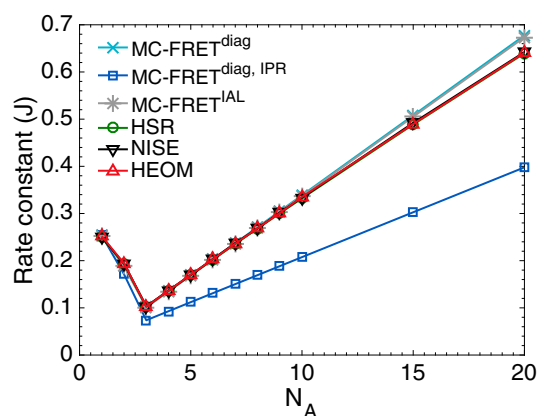


Fig. 3. Rate constant for the donor-acceptor energy transfer in the unbiased symmetric system as a function of N_A in the limit of high temperature and fast dynamics. The reorganization energy is fixed, $\lambda = 0.2 J$, resulting in $\kappa = 11.2$, and N_A varies from 1 to 20. All other parameters are the same as in Fig. 2.

4.2. High-temperature and slow-modulation limit

Next, we consider the regime of high temperature and move out of the fast-fluctuation regime (κ of the order of unity or smaller). The rate constant, calculated with the different methods applied to the symmetric system and compared to the HEOM method, are presented as a function of κ in Fig. 4. As can be seen from the plot, the methods deviate significantly from each other in this regime. First, when approaching the static limit, i.e., $\kappa, \Lambda \rightarrow 0$, the rate constant for the HSR method vanishes. This is in contrast to all the other methods and is a clear sign of the limitation of the HSR model to the white noise limit. The MC-FRET^{diag, IPR} consistently overestimates the rate predicted by the other methods. This can once more be attributed to overestimating the effect of exchange narrowing, resulting in too narrow lines, and thus higher rate constant. The NISE and MC-FRET^{diag} methods agree with the HEOM method over the whole range of κ , indicating that these methods both work well in this regime. While the MC-FRET^{IAL} gives results close to NISE and MC-FRET^{diag}, it gives an unreasonable absorption line shape in the slow dynamics limit: instead of giving a Gaussian with a FWHM $\sim \sigma$, which would be expected in the slow-modulation limit, Eq. 17 results in two Lorentzians of FWHM $\sim \Lambda$ when Λ decreases. This discrepancy is illustrated in Fig. 5, where the MC-FRET^{IAL} absorption line shape of the tetrameric acceptor is plotted together with the MC-FRET^{diag} absorption line shape and the emission line shape of the

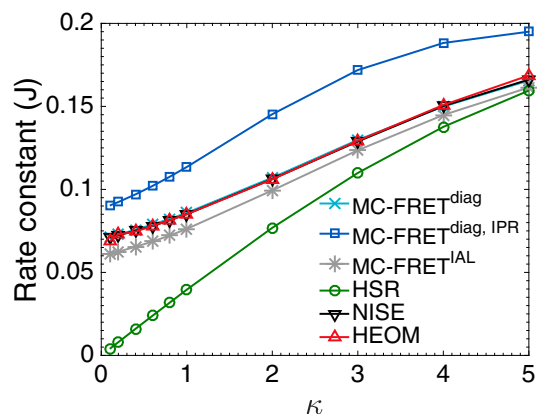


Fig. 4. Rate constant for the donor-acceptor energy transfer in the unbiased symmetric system with $J^A = 10 J$, $J^{D-A} = J$, and $N_A = 4$ as a function of κ in the limit of high temperature and approaching slow dynamics: $k_B T = 5000 J$, $\lambda = J$. The inverse of the correlation time Λ is varied from 10 to 500 J, resulting in κ from 0.1 to 5.0.

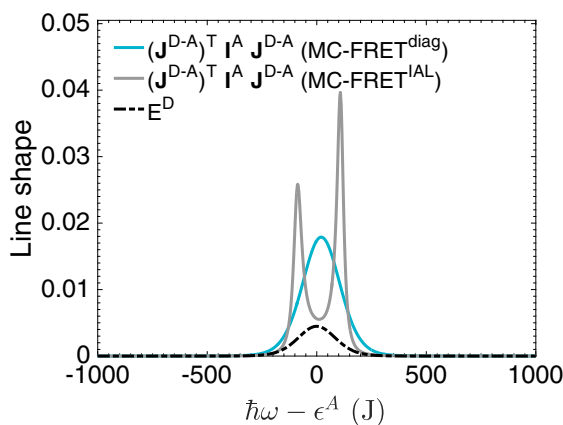


Fig. 5. Example of the unreasonable absorption line shape of the MC-FRET^{IAL} (solid gray line) of the tetrameric acceptor system compared to the MC-FRET^{diag} (solid blue line) method calculated for $\kappa = 0.4$. Both absorption line shapes include the donor-acceptor coupling, $(J^{D-A})^T I^A J^{D-A}$, therefore the rate constant is simply the overlap between these absorption line shapes and the emission line shape of the donor (dashed black line).

donor.

As the dynamics gets slow, Λ and κ decrease. In the static limit, the line width is proportional to σ and thus independent of Λ (see Eq. 10), and therefore it has a finite value. That is why the rate constant for all methods except the HSR model approaches a constant when κ approaches zero. For the HSR model, the rate approaches zero in the static limit, because the line shape in this method is given by a Lorentzian of width 2Γ . When Λ approaches zero, Γ gets very large (see Eq. 12) resulting in vanishing overlap, which in turn leads to a vanishing rate constant.

We now consider the effect of the size of the acceptor system on the rate constant calculated for biased symmetric systems and for one fixed value of κ , namely $\kappa = 0.4$. The results are presented in Fig. 6. Since $\kappa = 0.4$ corresponds to the regime of slow dynamics, HSR is not expected to be valid, and indeed a large deviation from HEOM is observed for all the graphs. From Fig. 6a ($\Delta E = 0$), it can be seen that the absolute deviation from HEOM for all methods is increasing with growing N_A . However, the relative error is independent of N_A (see Fig. S1 of SI). Having an energy bias between the donor and the acceptor molecules results in the shift of the excitonic energy levels relative to the donor excited state and hence influences the possible resonances. Therefore, by tuning the energy bias, the energy transfer can be either enhanced or suppressed. The energy bias also affects the agreement between the methods as can be seen especially for the case of the largest bias (Fig. 6c). The results can be understood from the fact that the absorption line shape differs for the considered methods: with no energy bias the overlap between the absorption and emission line shapes is largest due to the resonance (effect), hence discrepancies between the methods are largest; with a large energy bias, the overlap between the two line shapes is only partial, hence discrepancies are smaller, since the differences in the absorption line shapes are not as crucial as in the resonance case.

Next, we increase the nearest-neighbor interactions in the acceptor ring to $J^A = 150$ J compared to the donor-acceptor coupling, $J^{D-A} = J$, resulting in a much larger shift of the highest excitonic energy level for the acceptor. The other parameters are the same as in Fig. 6. From Fig. 7, it can be seen that the larger value of J^A generally results in a smaller rate constant than in Fig. 6, which directly results from the bad match between the energy of the donor with the acceptor's exciton band. The bump observed for $N_A = 2$ comes from the resonance effect discussed previously. This effect has more impact in systems of smaller size for larger coupling in the acceptor ring.

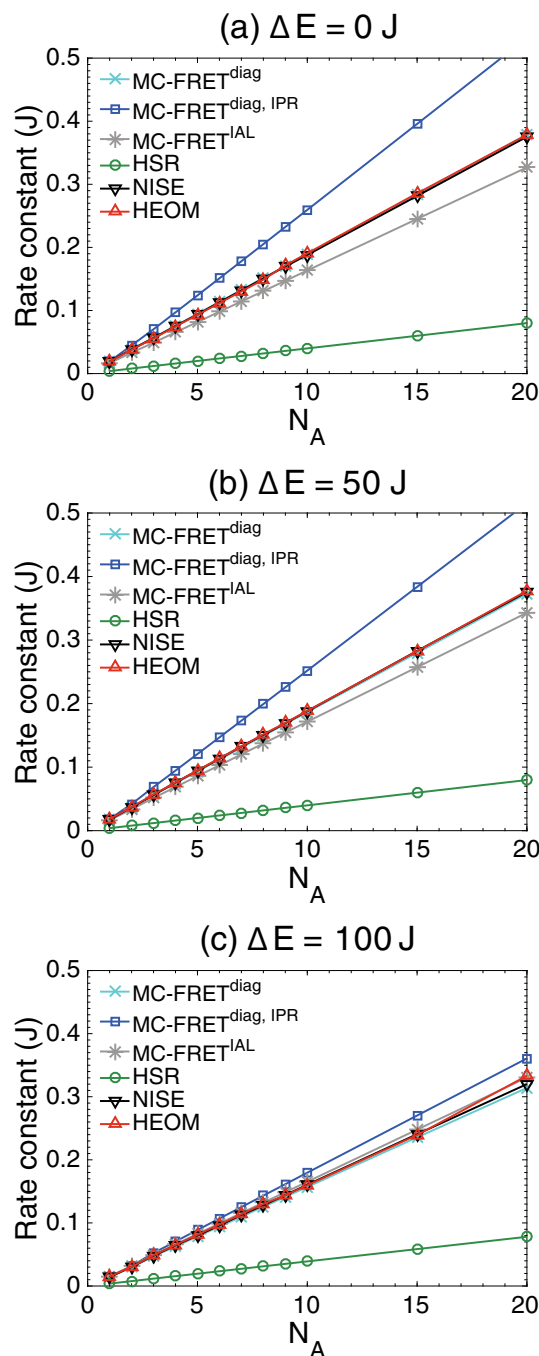


Fig. 6. Donor-acceptor rate constant for the energy transfer in the symmetric system as a function of N_A in the limit of high temperature and slow dynamics: $k_B T = 5000$ J, $\lambda = J$, $\Lambda = 40$ J resulting in $\kappa = 0.4$. Furthermore, $J^A = 10$ J, $J^{D-A} = J$, and N_A varies from 1 to 20. A different energy bias, ΔE , between the donor and acceptor molecular energies is used in the three panels.

Finally, we test the methods for the asymmetric system, where the donor molecule is coupled to only one of the acceptor molecules. We use the same parameters as for the symmetric system. Fig. 8 shows that all methods are in good agreement, except the HSR model, which fails to describe the slow dynamics of the bath. Thus, either of the MC-FRET or the NISE methods can be used in this case. It should be noted that unlike the symmetric case where the EET is dominated by transfer to the totally symmetric ($k = 0$) exciton state, in the asymmetric system all states within the exciton band participate. For small N_A (< 10), resonance effects appearing and disappearing due to the discrete positions of the exciton levels in the band, give rise to the observed

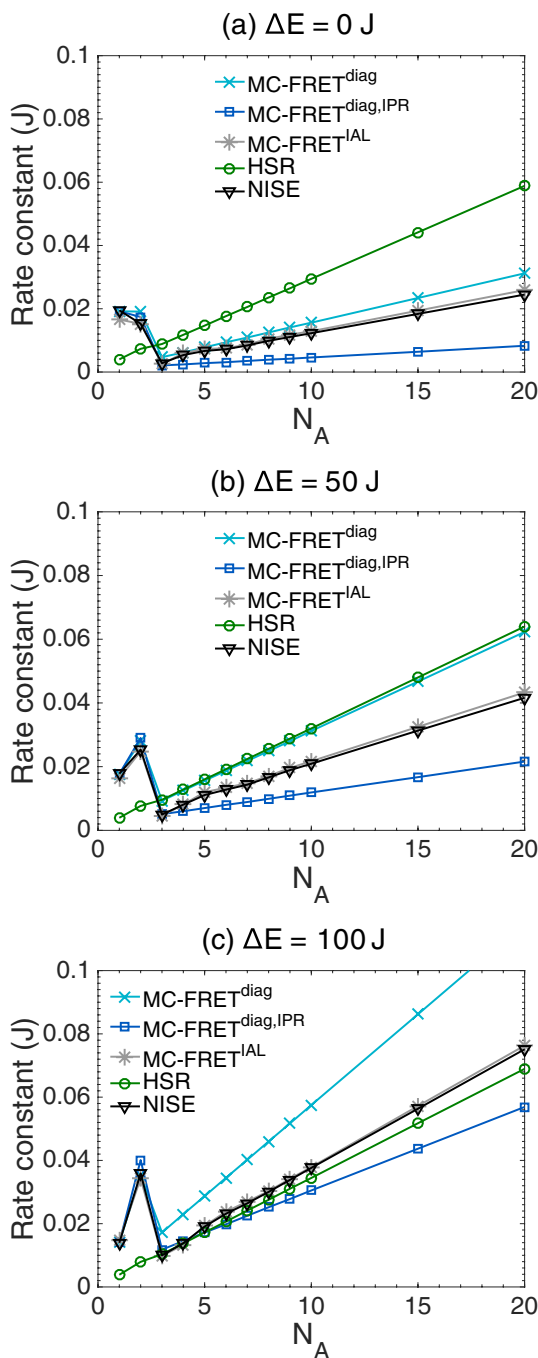


Fig. 7. Donor-acceptor rate constant for the energy transfer in the symmetric system as in Fig. 6, but now for a larger coupling within the acceptor ring, $J^A = 150 J$. All other parameters as in Fig. 6.

oscillations. By contrast, for the symmetric system such oscillations with N_A do not occur, as the predominant accepting state is the symmetric state, at fixed energy $\epsilon^A + 2J$ (unless $N_A < 4$). For large N_A , the rate constant almost does not change, because the addition of new exciton states does not change much the density of states and, therefore, hardly influences the overlap between the acceptor's absorption line shape and the donor's emission line shape. Furthermore, in the symmetric case, there are N_A couplings of magnitude J , resulting in the linear increase of the rate constant with the size of the acceptor's system. This is different from the asymmetric case, where there is only one coupling of magnitude J , and as a result the rate constant does not change with the increase of N_A .

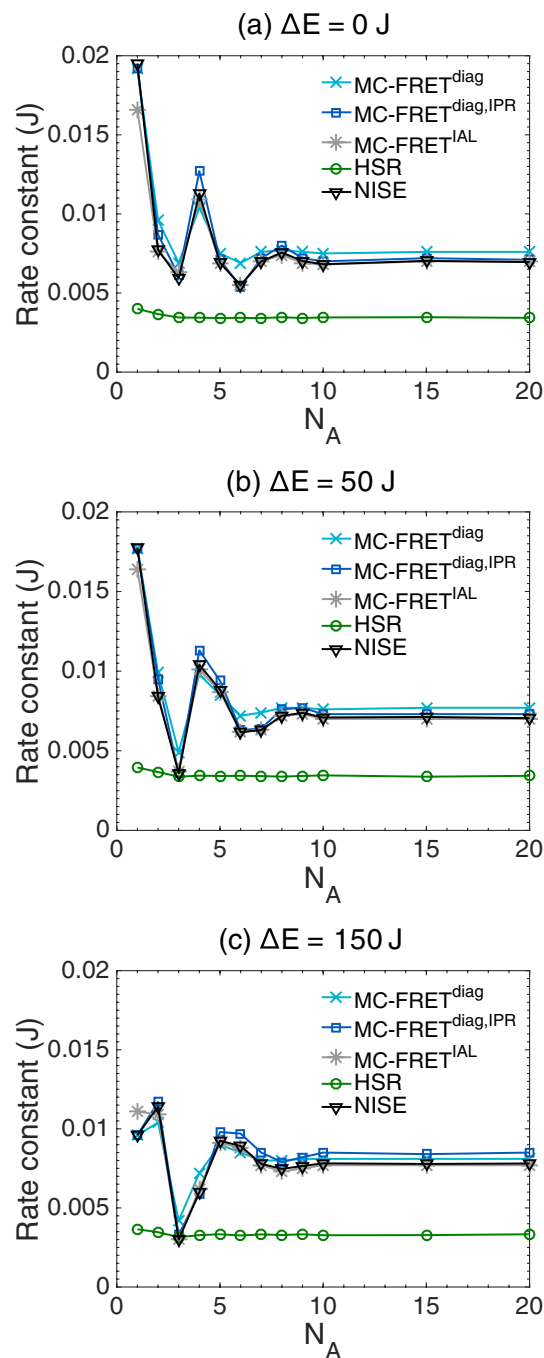


Fig. 8. Donor-acceptor rate constant for the energy transfer in the asymmetric system. All parameters as in Fig. 7.

4.3. Intermediate regime

The intermediate regime corresponds to the bath dynamics of many known light-harvesting systems, like, for example, LH2 [20,21], or self-assembled C8S3 nanotubes [28,30]. We chose the parameters close to those used previously for the LH2 system [51,72,73] (see Table 2) and apply them first to the symmetric system. Note that in this subsection, we use absolute units (cm^{-1} and ps^{-1}). The results for the rate constant in this parameter regime as a function of N_A are presented in Fig. 9a. Here, we compare them to the HEOM. The HSR method gives the worst results by overestimating all the rates except for the case $N_A = 1$. NISE and $\text{MC-FRET}^{\text{diag, IPR}}$ give the closest values for the rates to those of HEOM. NISE consistently predicts too high rates, while the other

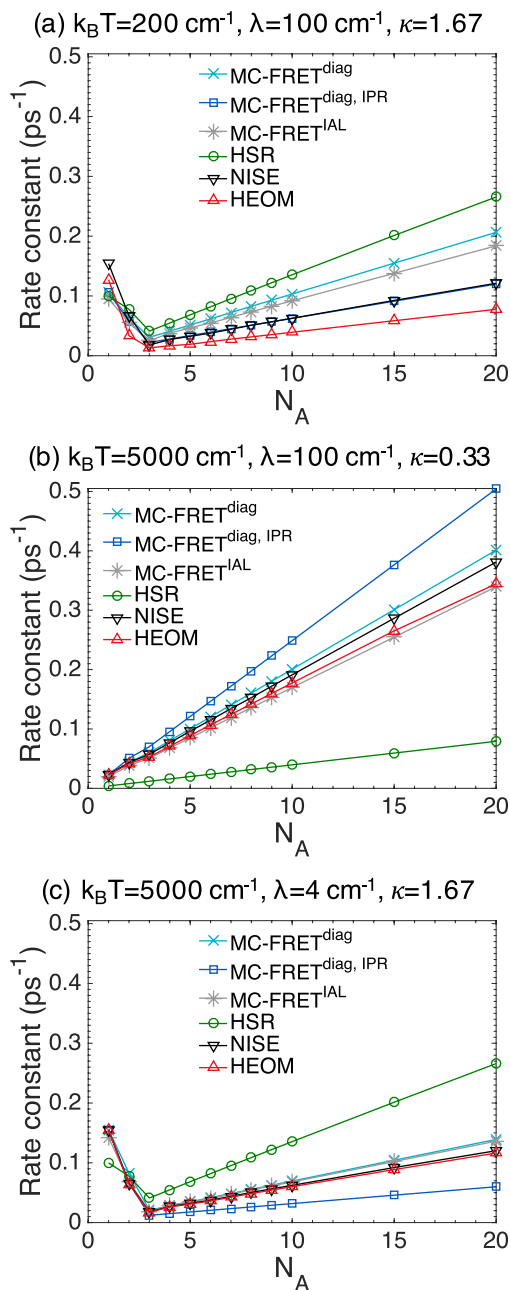


Fig. 9. Donor-acceptor rate constant for the energy transfer in the symmetric system in the range of LH2 parameters: $J^A = 300 \text{ cm}^{-1}$, $J^{D-A} = 20 \text{ cm}^{-1}$, N_A varies from 1 to 20; $\Lambda = 333.6 \text{ cm}^{-1}$. (a) Regime of room temperature; (b) high-temperature limit; (c) high-temperature limit and small reorganization energy.

methods predict too low rates for monomer to monomer transfer. MC-FRET^{diag} and MC-FRET^{IAL} give similar results and their predictions for the rate lie in between those for the HSR and the MC-FRET^{IAL} methods.

For better understanding the predicted results, we calculate the rate constant for the same system, except that we use the high-temperature limit ($k_B T = 5000 \text{ cm}^{-1}$), corresponding to $\kappa = 0.33$ (Fig. 9b), or alternatively use the high-temperature limit ($k_B T = 5000 \text{ cm}^{-1}$) and a low reorganization energy ($\lambda = 4 \text{ cm}^{-1}$, corresponding to $\kappa = 1.67$) (Fig. 9c). The results show that NISE is in good agreement with HEOM in both cases and has the lowest relative error compared to other methods (see SI). This confirms that its deviation from HEOM in the regime of parameters relevant to LH2 mainly comes from the high-temperature limitation. Here, MC-FRET^{diag} and MC-FRET^{IAL} give a rate

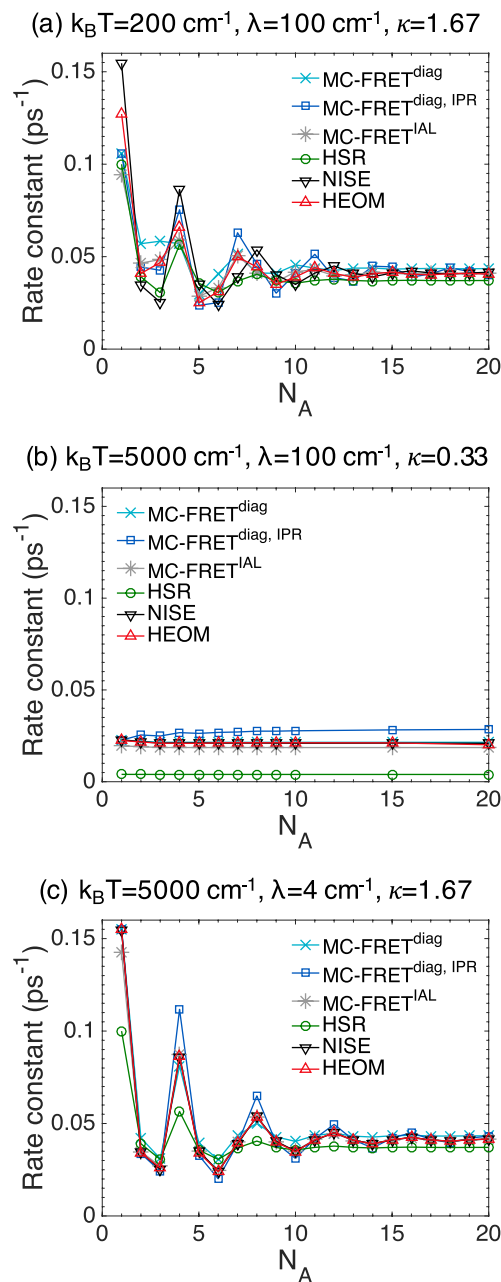


Fig. 10. Donor-acceptor rate constant for the energy transfer in the asymmetric system. The parameters are the same as in Fig. 9.

constant close to that of HEOM, while MC-FRET^{diag, IPR} overestimates the rate constant in Fig. 9b and underestimates it in Fig. 9c. This unpredictability is explained by the narrowness of the DOS line shape scaled by the IPR for the acceptor system compared to the line shape predicted by the other MC-FRET methods.

Again a resonance effect is observed around $N_A = 3$ and the same linear growth for large N_A , as discussed previously.

Finally, we consider the asymmetric system using the same parameters as for the symmetric system. The results are shown in Fig. 10. The observed resonance effect for the smaller acceptor size result from participation of all exciton states in the process of EET. Moreover, the overall rate constant for this configuration is lower than in the symmetric one, since in the latter there are more couplings, which increase the rate, as discussed previously.

The agreement between the methods is the same as for the symmetric system. However, the relative error is much lower. In this sense,

the HSR model becomes a good approximation for approximately $N_A > 10$ in the parameter regime of Fig. 10a and 10b.

The good performance of the NISE and HSR models found for room temperature for the symmetric and asymmetric systems should be expected to deteriorate if either λ or Λ is increased significantly compared to the temperature, as shown in Table 1. Therefore as temperature is lowered, these methods are expected to get worse both in the limits of fast and slow fluctuations. Similar effects will emerge in the MC-FRET based methods unless absorption and emission matrices correctly including these effects are used. Furthermore, if one were to generalize the methods to multichromophoric donor complexes, at low temperature the emission from the donor system will be collected in the lowest levels, breaking the high-temperature approximation of these methods.

5. Conclusions

In this paper, we compared different theoretical methods to study EET in molecular aggregates. The methods considered were the multichromophoric Förster resonance energy transfer (MC-FRET) approach (with three different approximations used for calculating the absorption line shape of the acceptor complex), the Numerical Integration of the Schrödinger Equation (NISE), and the Haken-Strobl-Reineker (HSR) model. We applied them to a system consisting of a monomeric donor coupled to a multichromophoric acceptor ring in a symmetric or asymmetric way. We tested the methods in a number of regimes and for certain parameter ranges we compared them against the “gold standard” Hierarchy of Equations of Motion (HEOM) method.

First, we verified that in the *high-temperature and fast-modulation limit*, all methods performed accurately, apart from MC-FRET^{diag}, IPR that failed to give correct results due to its overestimation of the exchange narrowing effect.

In the *high-temperature and slow dynamics limit*, the methods deviated considerably from each other. HSR then was clearly seen to fail as a result of the white-noise limit. MC-FRET^{diag}, IPR significantly overestimated the rate predicted by the other methods, again due to an overly pronounced exchange narrowing effect. MC-FRET^{IAL}, which uses the expression for the ideal absorption line shape based on the quantum master equation formalism [59,60], gave an unreasonable absorption line shape despite giving reasonable results for the EET rate. We found that MC-FRET^{diag}, which uses the diagonal approximation for the absorption line shape, agrees with NISE over the whole range of the inverse of the correlation time of the bath fluctuations, Λ . This suggests that MC-FRET^{diag} works well in this limit, since the NISE method has no limitations in this limit (its only limitation is its inherent high-temperature assumption).

In the *intermediate regime*, with bath dynamics comparable to that of many known natural light-harvesting systems, NISE gives the most reasonable results, though it systematically overestimates the rates predicted by HEOM. In this parameter regime, when looking at the high temperature limit, either MC-FRET^{diag}, MC-FRET^{IAL}, or NISE gives correct results. In the intermediate regime of the bath fluctuations, an accurate prediction of the line shape is at least as important as temperature effects. This explains the variability of the performance of different MC-FRET methods.

In the symmetric case, the donor predominantly couples to a single state of the acceptor complex – a totally symmetric exciton state ($k = 0$). This makes the description of the line shape of this state very critical: small changes in this line shape result in large variations of the rate constant. This explains the large sensitivity of the rate constant to the method used. In contrast, in the asymmetric case the donor couples to the whole exciton band. As a consequence, the line shape (of a single state) is not as critical anymore. This results in lower relative errors and hence less crucial dependency of the rate constant on the chosen method.

The MC-FRET methods showed to be by far the most computationally efficient. However, one should take into account that the

description of the line shape is crucial here. Studying exciton dynamics and energy transfer from a large multichromophoric donor to a large multichromophoric acceptor remains a big challenge. This can only be solved by implementing an accurate and efficient way of calculating the emission line shape function of the involved multichromophoric donor complexes. On the other hand, NISE being computationally more demanding, shows the most reasonable results despite its high-temperature limitation. In contrast to HEOM, it is straightforward to efficiently parallelize the NISE method.

Appendix A. Supplementary data

Supplementary data associated with this article can be found, in the online version, at <https://doi.org/10.1016/j.chemphys.2019.110478>.

References

- [1] G.D. Scholes, G.R. Fleming, A. Olaya-Castro, R. van Grondelle, *Nat. Chem.* 3 (2011) 763.
- [2] G.D. Scholes, G. Rumbles, *Materials For Sustainable Energy: A Collection of Peer-Reviewed Research and ReviewArticles from Nature Publishing Group*, WorldScientific, 2011, pp. 12–25.
- [3] F. Laquai, Y.-S. Park, J.-J. Kim, T. Basché, *Macromol. Rapid Commun.* 30 (2009) 1203.
- [4] F.M. Raymo, M. Tomasulo, *Chem. Soc. Rev.* 34 (2005) 327.
- [5] A.P. De Silva, H.N. Gunaratne, T. Gunnlaugsson, A.J.M. Huxley, C.P. McCoy, J.T. Rademacher, T.E. Rice, *Chem. Rev.* 97 (1997) 1515.
- [6] K. Szaciłowski, *Chem. Rev.* 108 (2008) 3481.
- [7] J. Wu, W. Liu, J. Ge, H. Zhang, P. Wang, *Chem. Soc. Rev.* 40 (2011) 3483.
- [8] T. Brixner, R. Hildner, J. Köhler, C. Lambert, F. Würthner, *Adv. Energy Mater.* 7 (2017) 1700236.
- [9] R. Croce, H. van Amerongen, *Nat. Chem. Biol.* 10 (2014) 492.
- [10] S.K. Saikin, A. Eisfeld, S. Valleau, A. Aspuru-Guzik, *Nanophotonics* 2 (2013) 21.
- [11] C. Curutchet, B. Mennucci, *Chem. Rev.* 117 (2016) 294.
- [12] H. Sumi, *J. Phys. Chem. B* 103 (1999) 252.
- [13] H. Haken, G. Strobl, *Zeitschrift für Physik A Hadrons Nuclei* 262 (1973) 135.
- [14] C. Liang, T.L.C. Jansen, *J. Chem. Theory Comput.* 8 (2012) 1706.
- [15] A. Ishizaki, Y. Tanimura, *J. Phys. Soc. Jpn.* 74 (2005) 3131.
- [16] D.E. Makarov, N. Makri, *Phys. Rev. E* 52 (1995) 5863.
- [17] V. Moulisová, L. Luer, S. Hoseinkhani, T.H. Brotsudarmo, A.M. Collins, G. Lanzani, R.E. Blankenship, R.J. Cogdell, *Biophys. J.* 97 (2009) 3019.
- [18] L. Luer, V. Moulisová, S. Henry, D. Polli, T.H.P. Brotsudarmo, S. Hoseinkhani, D. Brida, G. Lanzani, G. Cerullo, R.J. Cogdell, *Proc. Nat. Acad. Sci.* 109 (2012) 1473.
- [19] A.W. Roszak, T.D. Howard, J. Southall, A.T. Gardiner, C.J. Law, *Science* 302 (2003) 1969.
- [20] G. McDermott, S.M. Prince, A.A. Freer, A.M. Hawthornthwaite-Lawless, M.Z. Papiz, R.J. Cogdell, N.W. Isaacs, *Nature* 374 (1995) 517.
- [21] D.E. Chandler, J. Strümpfer, M. Sener, K. Schulten, *Biophys. J.* 106 (2014) 2503.
- [22] P. Jordan, P. Fromme, H.T. Witt, O. Klukas, W. Saenger, N. Krauß, *Nature* 411 (2001) 909.
- [23] Y. Umena, K. Kawakami, J.-R. Shen, N. Kamiya, *Nature* 473 (2011) 55.
- [24] N. Nelson, C.F. Yocum, *Annu. Rev. Plant Biol.* 57 (2006) 521.
- [25] G.T. Oostergetel, H. van Amerongen, E.J. Boekema, *Photosynth. Res.* 104 (2010) 245.
- [26] L.M. Günther, M. Jendry, E.A. Bloemsma, M. Tank, G.T. Oostergetel, D.A. Bryant, J. Knoester, J. Köhler, *J. Phys. Chem. B* 120 (2016) 5367.
- [27] Y. Wan, A. Stradomska, J. Knoester, L. Huang, *J. Am. Chem. Soc.* 139 (2017) 7287.
- [28] U. De Rossi, J. Moll, M. Spieles, G. Bach, S. Dähne, J. Kriwanek, M. Lisk, *J. Prakt. Chem.* 337 (1995) 203.
- [29] C. Spitz, J. Knoester, A. Ouart, S. Daehne, *Chem. Phys.* 275 (2002) 271.
- [30] D.M. Eisele, C.W. Cone, E.A. Bloemsma, S.M. Vlaming, C.G.F. van der Kwaak, R.J. Silbey, M.G. Bawendi, J. Knoester, J.P. Rabe, D.A.V. Bout, *Nat. Chem.* 4 (2012) 655.
- [31] S. Sengupta, D. Ebeling, S. Patwardhan, X. Zhang, H. von Berlepsch, C. Böttcher, V. Stepanenko, S. Uemura, C. Hentschel, H. Fuchs, F.C. Grozema, L.D.A. Siebbeles, A.R. Holzwarth, L. Chi, F. Würthner, *Angew. Chem. Int. Ed.* 51 (2012) 6378.
- [32] T. Förster, *Annalen der Physik* 437 (1948) 55.
- [33] L. Stryer, R.P. Haugland, *Proc. Natl. Acad. Sci. U.S.A.* 58 (1967) 719.
- [34] S. Jang, M.D. Newton, R.J. Silbey, *Phys. Rev. Lett.* 92 (2004) 218301.
- [35] G.D. Scholes, G.R. Fleming, *J. Phys. Chem. B* 104 (2000) 1854.
- [36] L. Banchi, G. Costagliola, A. Ishizaki, P. Giorda, *J. Chem. Phys.* 138 (2013) 184107.
- [37] J. Ma, J. Cao, *J. Chem. Phys.* 142 (2015) 094106.
- [38] J. Ma, J. Moix, J. Cao, *J. Chem. Phys.* 142 (2015) 094107.
- [39] J.M. Moix, J. Ma, J. Cao, *J. Chem. Phys.* 142 (2015) 094108.
- [40] A. Chenu, J. Cao, *Phys. Rev. Lett.* 118 (2017) 013001.
- [41] V.M. Kenkre, P. Reineker, *Exciton dynamics in molecular crystals and aggregates*, Springer tracts in modern physics, Springer, Berlin, 1982.
- [42] T.L.C. Jansen, J. Knoester, *J. Phys. Chem. B* 110 (2006) 22910.
- [43] C.P. van der Vegte, A.G. Dijkstra, J. Knoester, T.L.C. Jansen, *J. Phys. Chem. A* 117

- (2013) 5970.
- [44] Y. Tanimura, R. Kubo, *J. Phys. Soc. Jpn.* 58 (1989) 101.
- [45] A. Ishizaki, G.R. Fleming, *J. Chem. Phys.* 130 (2009) 234111 .
- [46] J. Strümpfer, K. Schulten, *J. Chem. Theory Comput.* 8 (2012) 2808.
- [47] A. Davydov, *Theory of Molecular Excitons*, Springer, US, 1971.
- [48] V.M. Agranovich, M.D. Galanin, *Electronic excitation energy transfer in condensed matter*, North-Holland Pub. Co., Amsterdam, 1982.
- [49] C. Olbrich, J. Strümpfer, K. Schulten, U. Kleinekathöfer, *J. Phys. Chem. B* 115 (2010) 758.
- [50] M. Agtar, U. Kleinekathöfer, C. Curutchet, B. Mennucci, *J. Phys. Chem. B* 121 (2017) 1330.
- [51] C.P. van der Vegte, J.D. Prajapati, U. Kleinekathöfer, J. Knoester, T.L.C. Jansen, *J. Chem. Phys. B* 119 (2015) 1302.
- [52] V. May, O. Kühn, *Charge and Energy Transfer Dynamics in Molecular Systems*, Wiley-VCH, 2000.
- [53] V. Czikkely, H.D. Försterling, H. Kuhn, *Chem. Phys. Lett.* 6 (1970) 11.
- [54] C. Didraga, A. Pugzlys, P.R. Hania, H. von Berlepsch, K. Duppen, J. Knoester, *J. Phys. Chem. B* 108 (2004) 14976.
- [55] M.E. Madjet, A. Abdurahman, T. Renger, *J. Phys. Chem. B* 110 (2006) 17268.
- [56] T. Renger, *Photosynth. Res.* 102 (2009) 471.
- [57] S. Mukamel, *Principles of Nonlinear Optical Spectroscopy*, Oxford University Press, New York, 1995.
- [58] R. Kubo, *Stochastic Processes in Chemical Physics*, K.E. Shuler (Ed.), *Adv. Chem. Phys.* vol. XV, JohnWiley and Sons, New York, 1969, p. 101.
- [59] S. Jang, M.D. Newton, R.J. Silbey, *J. Phys. Chem. B* 111 (2007) 6807.
- [60] S. Jang, R.J. Silbey, *J. Chem. Phys.* 118 (2003) 9324.
- [61] K. Mukai, S. Abe, H. Sumi, *J. Phys. Chem. B* 103 (1999) 6096.
- [62] P.-W. Anderson, P.R. Weiss, *Rev. Mod. Phys.* 25 (1953) 269.
- [63] H. Sumi, *J. Chem. Phys.* 67 (1977) 2943.
- [64] E.W. Knapp, *Chem. Phys.* 85 (1984) 73.
- [65] H. Fidder, J. Knoester, D.A. Wiersma, *J. Chem. Phys.* 95 (1991) 7880.
- [66] L. Cleary, J. Cao, *New J. Phys.* 15 (2013) 125030 .
- [67] D.J. Thouless, *Phys. Rep.* 13 (1974) 93.
- [68] D. Cringus, T.L.C. Jansen, M.S. Pshenichnikov, D.A. Wiersma, *J. Chem. Phys.* 127 (2007) 084507 .
- [69] C. Leforestier, R.H. Bisseling, C. Cerjan, M.D. Feit, R. Friesner, A. Guldberg, A. Hammerich, G. Jolicard, W. Karrlein, H.D. Meyer, N. Lipkin, O. Roncero, R. Kosloff, *J. Comput. Phys.* 94 (1991) 59.
- [70] <https://www.ks.uiuc.edu/research/phi/>.
- [71] M. Wubs, J. Knoester, *Chem. Phys. Lett.* 284 (1998) 63.
- [72] O. Rancova, J. Sulskus, D. Abramavicius, *J. Phys. Chem. B* 116 (2012) 7803.
- [73] Y.-Z. Ma, R.J. Cogdell, T. Gillbro, *J. Phys. Chem. B* 101 (1997) 1087.